UCRL--93261

DE86 010980

Electrical Measurement Techniques for Pulsed High Current Electron Beams

K.W. Struve

This paper was prepared for submittal to
Measurement of Electrical Quantities
in Pulse Power Systems-II
National Bureau of Standards
Gaithersburg, Maryland
March 5-7, 1986

April 1, 1986

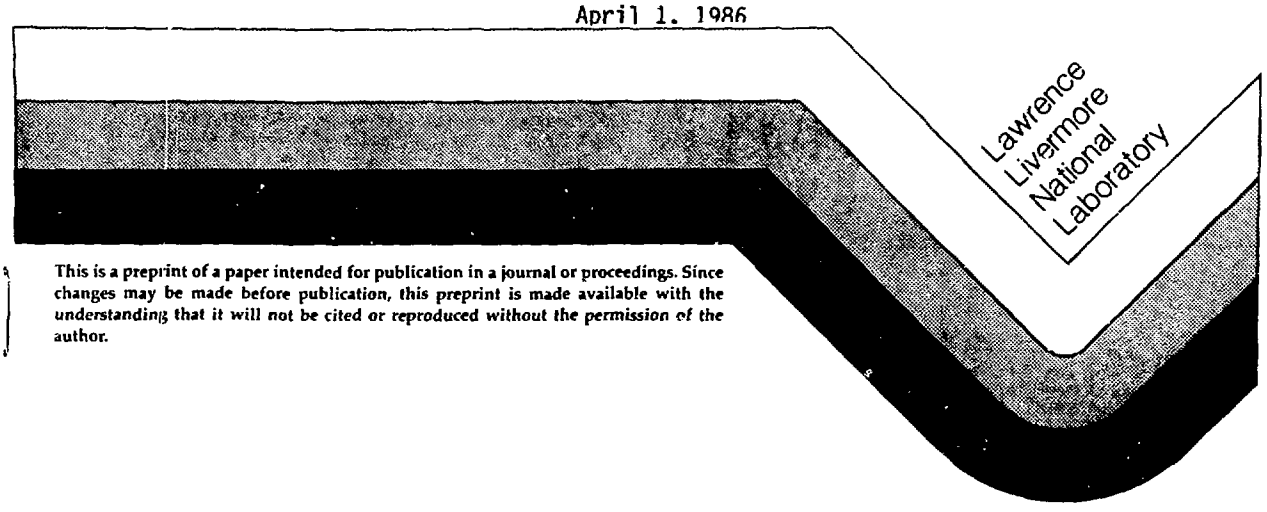

ELECTRICAL MEASUREMENT TECHNIQUES FOR PULSED HIGH CURRENT ELECTRON BEAMS

K. W. Struve

Lawrence Livermore National Laboratory
Livermore, California 94550

Abstract

The advent of high current (1 to 100 kA), moderate energy (> 10 MeV), short pulse (1 to 100 ns) electron accelerators used for charged particle beam research has motivated a need to complement standard diagnostics with development of new diagnostic techniques to measure electron beam parameters. A brief survey is given of the diagnostics for measuring beam current, position, size, energy, and emittance. While a broad scope of diagnostics will be discussed, this survey will emphasize diagnostics used on the Experimental Test Accelerator (ETA) and Advanced Test Accelerator (ATA). Focus is placed on diagnostics measuring beam current, position and size. Among the diagnostics discussed are resistive wall current monitors, B_θ loops, Rogowski coils, Faraday cups, and x-ray wire diagnostics. Operation at higher current levels also increases radiation and electromagnetic pulse interference. These difficulties and methods for circumventing them are also discussed.

Introduction

In the charged particle beam propagation program the major machines in use are the ETA [1] and ATA [2] at the Lawrence Livermore National Laboratory, and the RADLAC II [3] at Sandia National Laboratory. The ATA is a 10 kA, 50 MeV electron linear induction accelerator which is Blumlein charged and is typically fired at a rate of 1 Hz. The RADLAC II is a 40 kA induction accelerator which is Marx bank charged and typically fired four to six times per day. Other lower energy, single shot machines have been used in supporting experiments and for developing diagnostics. In this paper I discuss some of the electrical diagnostics used with these machines. In most cases the diagnostics are new uses of old techniques. However there are some new regimes and improvements that can be of use to a broader community.

I restrict my discussion to non-optical diagnostics except to mention that some very useful information can be gained from the Cerenkov radiation and transistion radiation from beam-intercepting foils, and from the optical emission of the beam produced plasma [4]. Witness plates have also been used extensively with some of the single shot machines, but they give only time integrated beam size measurements. They are often difficult to interpret because of limited dynamic range. Also neglected are interferometric techniques, which can give gas densities, plasma densities, and conductivities [5].

General Considerations

Typical parameters of interest in the particle beam program are risetimes ranging from subnanoseconds to tens of nanoseconds, current amplitude ranging from 1 A to greater than 10 kA, and energy up to 50 MeV. The ATA x-ray dose rate has been measured in excess of 10^{10} rad/sec, and neutron production of 10^{12} neutrons/pulse. These factors have especially complicated some of the lower current measurements. Typical radiation signals induced in cables on the ATA are seen in Fig. 1. The heliax cables exhibit a negative noise spike corresponding to a Compton electron current in the cable, which has been seen to be as large as 5 V. The braided outer conductor

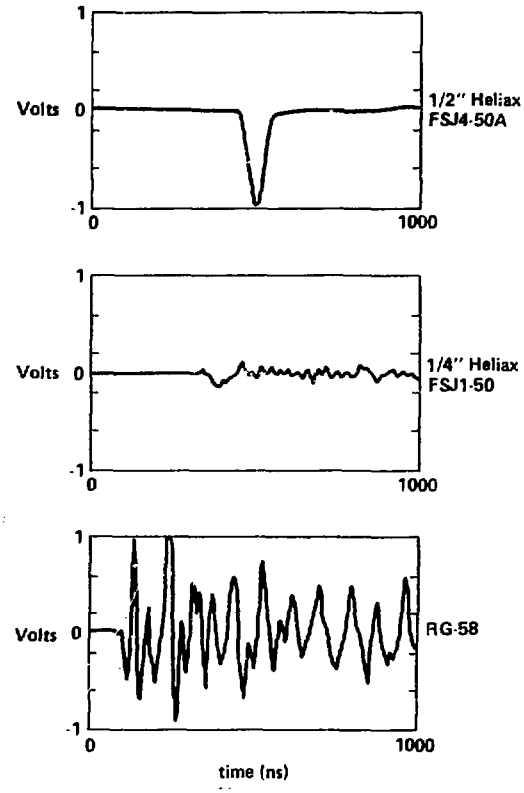

Figure 1. Typical radiation induced cable noise for three cable types with a dose of 2000 rad-cm.

cables, such as RG-58, pick up a severe x-ray induced electromagnetic pulse (EMP) interference signal. Both of these effects are well known [6,7]. They can be minimized by proper choice of cable type, by limiting cable lengths in areas of intense radiation, and by using diagnostics with a large output voltage. This last requirement, for example, suggests that it is preferable to integrate B_θ signals outside the radiation environment. The best cable type has a small diameter, solid outer conductor and a high density dielectric. The compromise, however, is higher attenuation as cable diameter is reduced. A summary of both Compton electron signal and EMP signal induced noise amplitudes versus cable type as measured on the ATA is shown in Fig. 2.

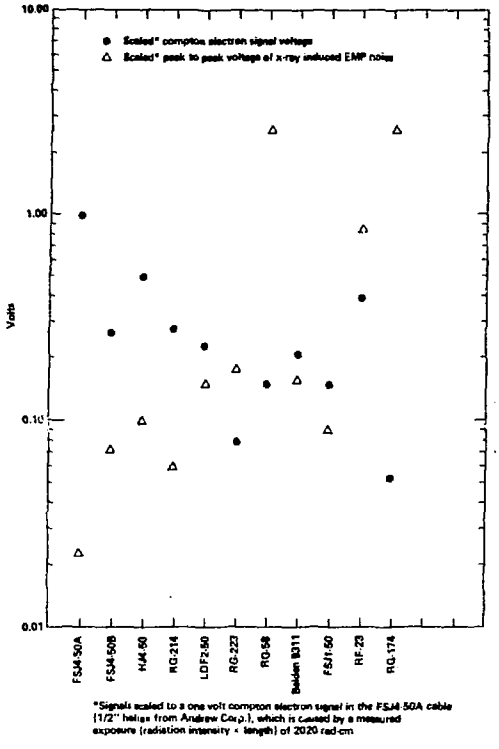

Figure 2. Amplitude of radiation produced noise for several cable types with an x-ray dose of 2000 rad-cm.

In spite of these concerns, electrical diagnostic techniques have been used to measure beam current, net current, beam current density, beam energy, position, size, and emittance. Some of these different techniques are summarized in Table 1. Beam and net current measurements, beam centroid position measurements, and beam size measurements are discussed in more detail in the next section.

The distinction is made between beam and net current measurements in Table 1 because return currents can flow in the plasma surrounding the beam propagating in gas. The sum of the beam and plasma current is the net current, as shown in Fig. 3. A return current also flows in the conducting wall which is equal in magnitude to and opposite in direction to the net current. It results from the vanishing magnetic field at the wall. Therefore, any diagnostic at the wall which measures either the wall return current or the magnetic field of the beam is actually measuring the net current and not the beam current. For pressures and pulse lengths $p\tau < 2$ Torr-ns in air (pressure x pulse length) the plasma current is negligible and the net current equals the beam current [8]. For higher pressures plasma currents can strongly contribute to the net current both during and after the pulse. Also important is the radial profile of both the plasma and beam current densities since they determine the magnetic field within the beam and hence the radial forces acting on the beam electrons. An effective current is sometimes defined from these profiles to describe the average effect of the plasma current on the beam electrons.

Table 1.

Survey of electrical diagnostic techniques used in the electron beam propagation program.

Diagnostic	Quantities measured	Comments
Wall current monitor	I_{net} (t); $\Delta x, \Delta y$(t)	τ_r = 0.3 ns, τ_d >2 μsec
Rogowski coil	I_{net} (t)	τ_r ≈ several ns, needs integrator
Sine cosine coil	Δx, Δy (t)	τ_r ≈ several ns, needs integrator
Frost monitor	I_{beam} (t); Δx, Δy(t)	τ_r < 1 ns, needs integrator. Can be damaged with multiple shots
$\hat{B}_{\theta}$ loop	I_{net} (t); Δx, Δy(t)	Gives I_{net} when integrated. Useful for high freq. (up to 2 GHz)
$\hat{B}_{\theta}$(r) probe	I_{beam} (t); r(t)	Can be used to meas. J_{plasma} when inserted into beam
Faraday cup	I_{beam} (t), r(t)	Beam profile when scanned, τ_r < 1 ns
Energy analyzer	E(t)	Bending magnet and slit combination. 1% energy variation, 1 ns resolution
X-ray probe	r(t)	0.3 ns, 1.5 mm resolution; requires repeatable shots
	ε(t)	Vacuum free expension, 0.3 ns
Electric probe	e(t)	1 ns, 3 mm resolution; requires unfolding and repeatable shots
Emittance mask	ε(t)	5 ns resolution; E_{beam} < 10 MeV
Emittance collimator	ε(t)	1 ns resolution; 2 MeV < E_{beam} < 50 MeV Requires B_z field and collimator dia. to match emittance range

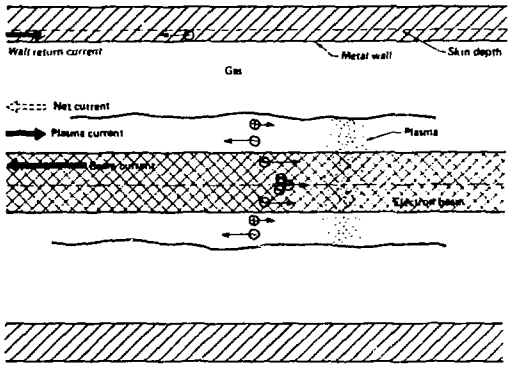

Figure 3. Beam current vs. net current vs. wall return current. Cross-section of an electron beam being transported through a gas filled drift chamber.

Beam energy has typically been measured on the ATA by sampling a small portion of the beam current and observing its transport through a bending magnet, slit, and current measuring device [9,10]. By varying the field strength of the bending magnet and accumulating many pulses it is possible to unfold beam energy versus time with several nanosecond resolution.

Beam emittance is a measure of the transverse velocity spread of the beam. It has been measured on the ETA with an emittance mask [11], a collimating aperture immersed in an axial magnetic field [12], and by measuring the size at several axial locations of a

beam freely expanding in vacuum [13]. The emittance mask technique is not practical with the higher energy of the ATA, but the other two techniques have been used.

Specific Diagnostics

Resistive Wall Current Monitor

Resistive wall current monitors (called beam bugs in the Livermore jargon) have been used with the ETA and ATA to measure beam current and position in vacuum, and net current in gas. They consist of a 0.13 mm thick, 25 mm wide stainless steel foil (alloy 304) welded to a stainless steel flange. When inserted in the beamline the foil becomes the beamline wall and functions as a voltage dropping resistor. An earlier version used on the ASTRON accelerator used discrete carbon resistors [14]. It was considerably more sensitive to noise. The construction of the ATA wall current monitor is shown in Fig. 4. The voltage

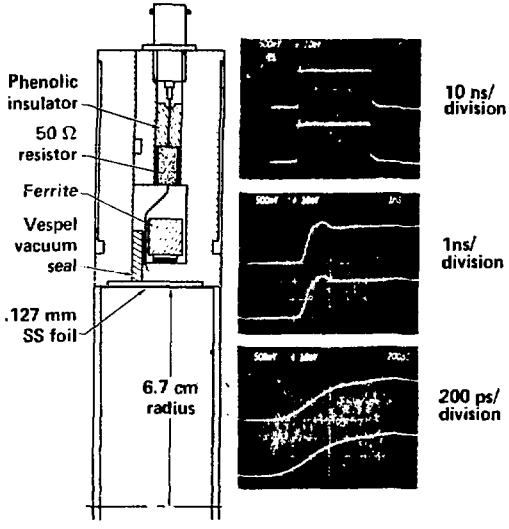

Figure 4. The ATA resistive wall current monitor. In each oscillogram the upper signal is the input at 10 A/div, and the lower is the response at 10 mV/div. The calibration is 1.0 kA/volt.

drop across the foil appears across the two halves of the device and is prevented from shorting out by the ferrite inductor. The ferrite also allows inverting the signal by bringing the lead around the back side of ferrite and attaching to the other side of the gap. The vacuum seal is made with a polyimide washer which also electrically insulates the two halves of the flange. Beam current is determined by monitoring the voltage drop across the foil at eight azimuthally symmetric locations. Four of the pickoffs are averaged to provide a signal proportional to the beam current, as shown in Fig. 5. The voltage drop around the foil is a function of the position of the beam centroid.

$$V(\theta) = kI \frac{1 - \rho^2}{1 + \rho^2 - 2\rho \cos\theta} \equiv kIF(\rho,\theta) \quad , \qquad (1)$$

where ρ is defined as the centroid offset normalized to the pipe radius. For convenience ρ is taken in the x direction only. The constant k is the calibration and includes the attenuators shown in the figure. When the outputs at 45°, 135°, 225°,

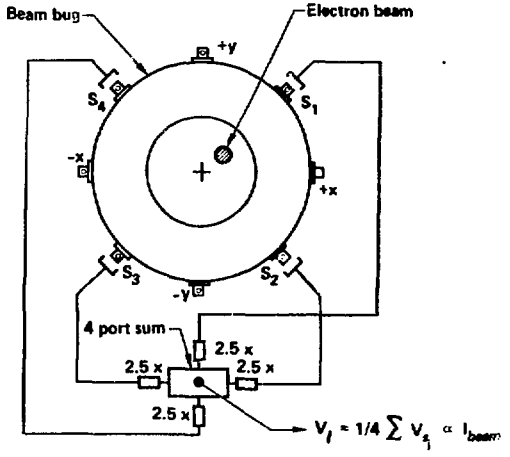

Figure 5. Cabling of the beam current monitor for beam current.

and 315° are summed for small ρ the result is $V_I = k\,I$, which is independent of ρ to second order. Beam centroid position is determined as shown in Fig. 6 by summing two opposing outputs. In the x direction for small ρ, $V_x = 1/2\,[V(180^\circ) - V(0^\circ)] = 2V_I\,\rho$. Note that for this choice of ρ, $V_y = 0$. For $\rho \geq 0.5$ these simple formulas are no longer good approximations. As ρ approaches one, Eq. 1 also becomes no longer valid because there can be significant beam loss to the walls.

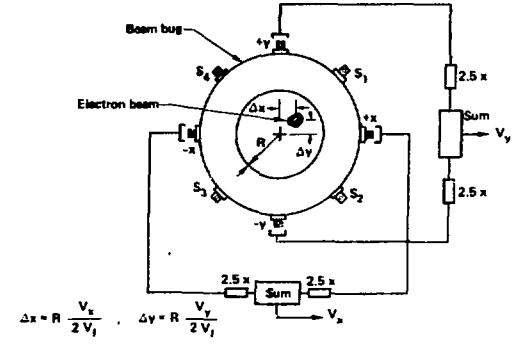

Figure 6. Cabling of the beam current monitor for beam position.

The calibration of the ATA accelerator current monitor is 1.0 kA/volt. Its risetime is 0.3 ns, and its L/R decay time is greater than 10 μs. The calibration is determined in a 50 Ω transmission line which matches the current monitor in size. A 1000 V, 0.5 ns rise pulse is sent through the line, and the output voltage of the monitor recorded. These traces are also shown in Fig. 4. A typical beam current signal is seen in Fig. 7. The x and y

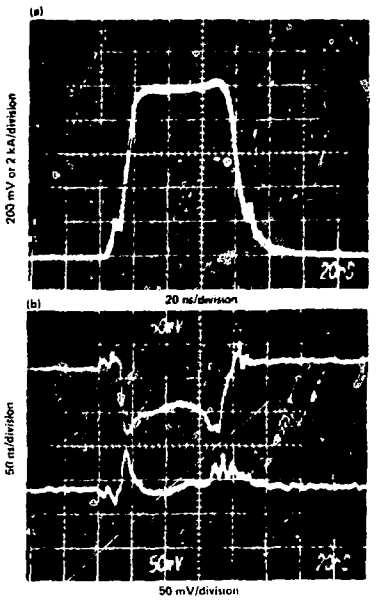

Figure 7. Typical current, and x, y signals from an ATA resistive beam current monitor. The signals have been attenuated ten times.

positions of the beam centroid must be determined by dividing by the current at each time in the pulse. Near the head and tail of the pulse large division errors can result if the traces are not correctly aligned.

Since 5% carbon resistors are used in the construction of the monitor and the summing circuits, absolute position cannot be determined to better than ± 5% of the pipe radius. In practice the resistors may vary 5% from the nominal value but only 1 to 2% from each other in a batch. By careful choice of resistors these errors can be minimized. Also, even though the absolute position may be uncertain, the relative time-varying position measurement is limited only by the noise level of the signal. Typically, relative displacements of 0.1% of the pipe radius are measured.

One other important limitation should be noted. That is, the resistive monitor should not be used near dipole or quadrupole magnetic fields since these fields will be badly distorted by the ferrite inductor. However, the monitor has been used within the axial field of a focusing solenoid with no ill effect on either beam transport or performance of the diagnostic.

When the current monitor is used in areas of large x-ray background, there is a large noise signal produced in the diagnostic cabling, as seen in Fig. 8. The cabling for this monitor was routed upstream before leaving the radiation area. Radiation from beam spill ahead of the current monitor reached the cable before the beam current signal causing the noise signal to appear ahead of the pulse. If the beam spill had occurred near the current monitor it would have been more difficult to detect.

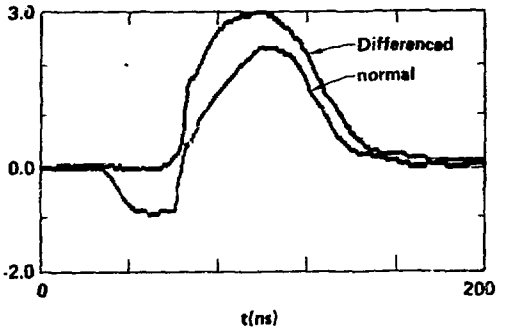

Figure 8. Beam current signal distorted by x-ray induced noise shown overlayed with the same signal differenced to reduce noise.

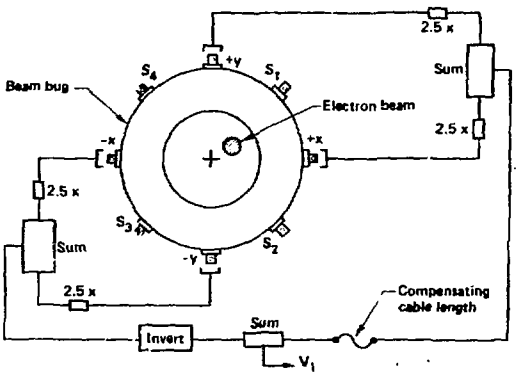

Figure 9. Differencing scheme for the current monitor.

By changing the cabling to difference out the x-ray signal as shown in Fig. 9 it was possible to practically eliminate the radiation noise. To properly subtract out the x-ray signal requires equalizing cable lengths to within 100 ps, routing the cables along the same path so that they all receive the same x-ray flux, inverting the signal from a negative ports, and adding to the output of a positive ports. In a similar manner new x and y signals can be constructed from the S ports.

Faraday Cups

Small aperture Faraday cups have been used with high current electron beams to determine beam profiles and current [15]. For energies above a few hundred keV the primary electron range in the current collector is sufficiently large that secondary electron loss from the collector is small. This eliminates the need for elaborate secondary emission suppression grids. High frequency response is obtained by building the Faraday cup into a 50 Ω transmission line, as done by Lauer [16] and shown in Fig. 10. Unless the total beam current is limited with an aperture very large voltages can develop causing internal arcing. The aperture diameter also determines the spatial resolution of the measurement. Current density is determined by scanning the diagnostic through the beam and recording signal amplitude as a function of time and position. A

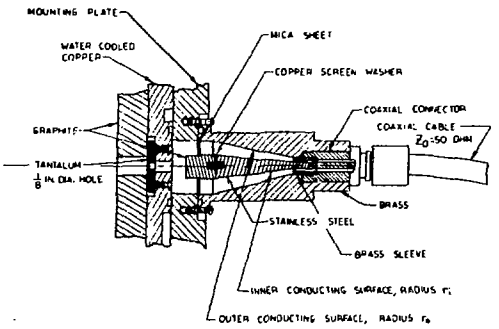

Figure 10. ETA 50 Ω fast Faraday cup.

device that has been used on the ETA to scan the Faraday cup is shown in Fig. 11. The center collector of the Faraday cup, and the aperture would need to be constructed of carbon and substantially thickened to survive the 50 MeV ATA beam.

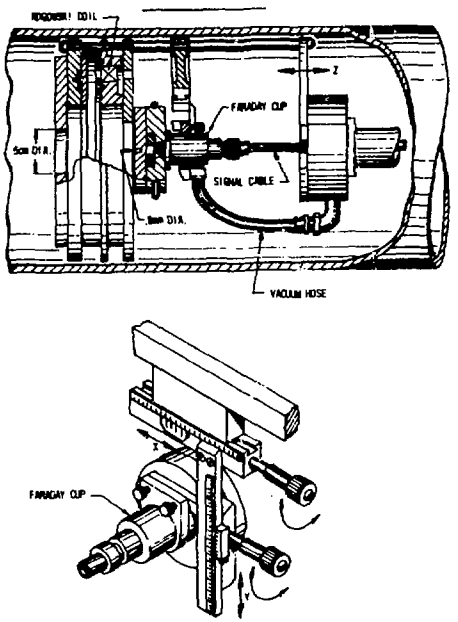

Figure 11. ETA xyz Faraday probe.

Beam profile measurements can also be made with single shot machines by use of a Faraday cup array [17]. A particulary inexpensive version has been constructed by Ekdahl [18]. It consists of a bundle of semi-rigid cables assembled and held together with a binder. The face of the bundle is machined flat, and the assembly oriented towards the beam. The center conductor of each cable acts as a small Faraday cup. The assembly will not withstand many shots but it does enable time and spatially resolved beam current measurements.

B_θ Loops

B_θ loops can be used to measure beam position, current, and high frequency transverse motion. The voltage induced in a single turn loop located at the wall is $-d/dt(B_\theta A_p \alpha)$. The probe area is A_p and the magnetic field B_θ is

$$B_\theta = \frac{\mu_0}{2\pi R} I F(\rho,\theta) \quad . \tag{2}$$

A factor α is included to account for the geometrical shielding of the probe by the port through which it is inserted. This factor must be determined empirically. It is typically of order 1/2. The beamline radius is R. The electrically shielded B_θ probe used on the ATA is shown in Fig. 12.

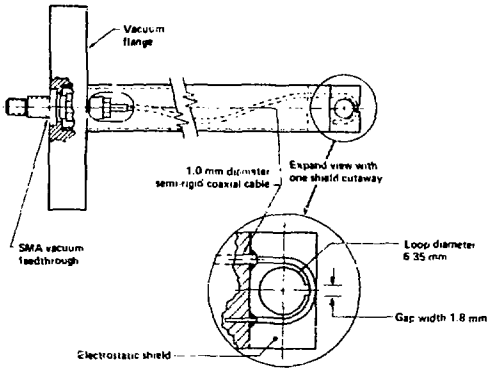

Figure 12. ATA shielded B_θ probe.

Besides electrically shielding the loop, the metal shields shown also precisely determine the loop area. This probe is normally used to measure high frequency (up to several GHz) transverse beam centroid motion. For sinusoidal motions, neglecting dI/dt, its output voltage at a frequency f is

$$V_{probe} = 4\pi f\, k\, I \cos\theta\, \Delta R_{max}/R^2 \quad , \tag{3}$$

where ΔR_{max} is the oscillation amplitude, and θ the plane of oscillation. In mks units the constant k is $\mu_0 A_p \alpha/2\pi$. A typical signal is shown in Fig. 13. The large signals at the head and tail of the pulse are due to the current rise and fall. The 800 MHz oscillations in the middle are caused by beam centroid motion.

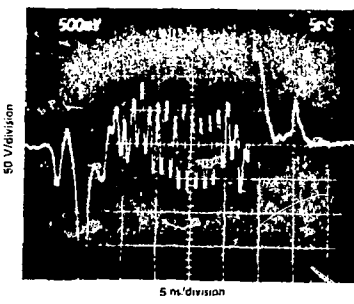

Figure 13. Typical B_θ loop signal.

With the Mirnov [19] configuration sets of opposing probes are cabled as shown in Fig. 14. The resulting output is proportional to the time derivative of IΔR. That is,

$$V_x = 2\frac{k}{R}\cos\theta\,\frac{d}{dt}(I\rho) \qquad (4)$$

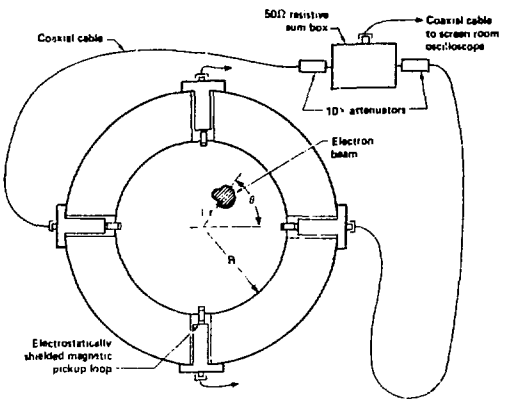

Figure 14. B_θ loops used to measure IΔR.

For those times in the pulse where dI/dt is small, the output is proportional to the beam position. However, the technique is also useful for directly measuring the excitation levels of the beam breakup instability, which for the ATA is the 800 MHz component of the product IΔR [20].

When the signals from four probes oriented in the same direction are summed, the result is a signal proportional to the time derivative of the net current. This configuration is equivalent to a Rogowski loop encircling the beam, except that the pulse risetime is not limited by the signal propagation time around the beamline as it is with a Rogowski coil.

An alternative approach to using discrete B_θ loops is to construct an inductive loop in the beamline wall, as shown in Fig. 15. The loop becomes a current viewing inductor. When the gap in the wall is filled with a dielectric that extends completely across the beamline, the plasma return current is forced to flow around the inductor. The magnetic flux of the loop, and hence the output signal, is then proportional to the beam current, and not the net current. This device was first built by Frost [21]. Its biggest advantage is that it can directly measure beam current. Its major limitation for multiple shot machines is the survivability of the dielectric.

One other interesting B_θ probe is one developed by Carlson and Stout [22]. It consists of a single turn loop which is self integrating. It has a risetime of < 200 ps and an L/R decay time of 64 ns. Its integrating resistor is a nickel-plated ceramic radial resistor. The value of the resistor is precisely controlled during the nickel plating process to give the desired calibration.

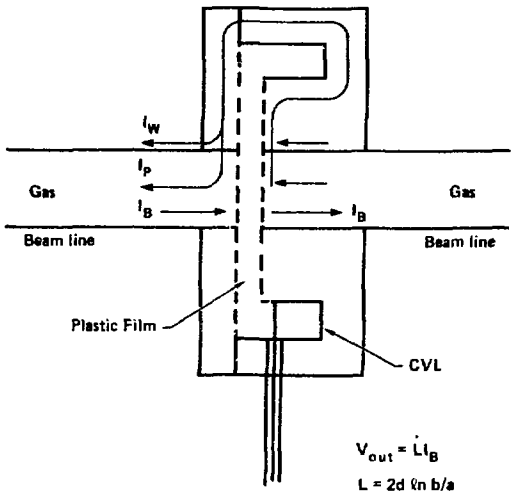

Figure 15. Frost monitor. Current viewing inductor with dielectric for beam current measurement.

Rogowski Loops

Rogowski loops have been used primarily with the single shot machines in the electron beam propagation program. They perform essentially the same measurement as summed B_θ loops except that with many more turns their sensitivity can be much higher. They have been used in both the self-integrating and the differentiating modes. In the integrating mode a low inductance resistor is placed across the output. A discussion of the technique is found elsewhere [23]. Analysis has shown that when the coil is wound back on itself to reduce the B_z pickup, or when it has an electrostatic shield there exists sufficient capacitance to ground that a transmission line approach must be applied [24,25].

Some of the advantages of Rogowski loops are that they are inexpensive to construct, they have a much higher signal than B_θ loops and are thus less sensitive to noise when many more turns are used, and that they are insensitive to positioning. Some of the disadvantages are that the signal must be integrated, the risetime is a function of the signal propagation time around the loop and can become severly degraded if larger diameter loops are used, and that ringing occurs if the beam is off-center. Also no centroid position indication is given unless the winding density varies as the cosine of the angle around the loop as shown schematically in Fig. 16. Ekdahl has used sine-cosine coils to give centroid position with high current electron beam accelerators [26]. He has shown that it is possible to replace the continuously varying winding density with a finite number of discrete multiturn loops connected in series.

For subnanosecond resolution of beam current and position it is necessary to replace the Rogowski coil with individual B_θ loops placed as shown in Fig. 16. They must be summed and integrated externally with care being taken to keep cable lengths matched so that phase shift errors are not introduced.

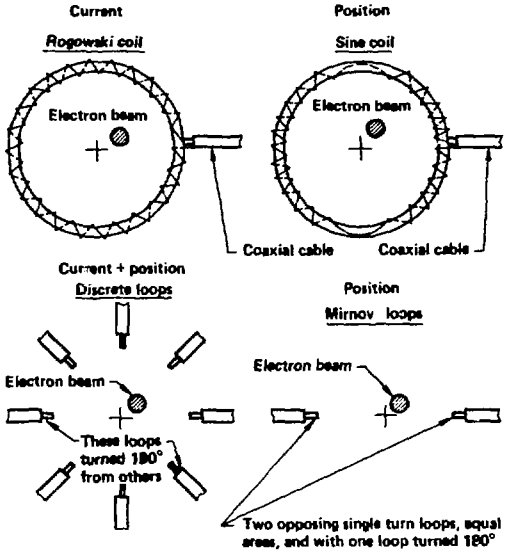

Figure 16. Comparison of Rogowski coils and B_θ loops for beam current and position measurements.

RC Integrators

Fast, high impedance RC integrators, which must be used at the oscilloscope and not within the transmission line, are commercially available [27]. To minimize the loss of high frequency components of an unintegrated B_θ or Rogowski loop signal, for example, it is desirable to integrate just outside the area of high noise level before significant attenuation has occurred. Frost [28] has built a 50 Ω integrator with a low inductance barium titanate chip capacitor that has a subnanosecond risetime and a 1.0 μsec decay constant. Its circuit is shown in Fig. 17. The output for $t \ll \tau$ is

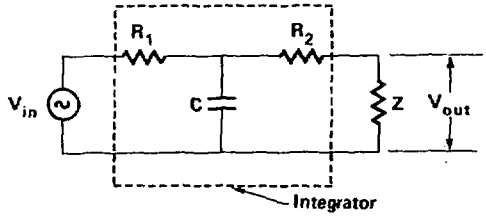

Figure 17. Schematic of RC integrator.

$$V_{out} = \frac{Z}{\tau R_1} \int_0^t V_{in}(t)dt \quad , \qquad (5)$$

where $\tau = (R_2+Z)R_1C/R_T$ and $R_T = R_1+R_2 = Z$. For the 50 Ω integrator $R_1 = R_2 = Z = 50$ Ω, $\tau = 2/3\ ZC$, and $Z/R_T = 1/3$. For a high impedance integrator where $R_2 = 0$ and $Z \gg R_1$, $\tau = r_1C$ and $Z/R_T = 1$. The obvious advantage of the high impedance integrator is that a smaller capacitor can be used to obtain the same time constant. However, by using a barium titanate capacitor in a low inductance configuration as shown in Fig. 18, comparable decay times and higher

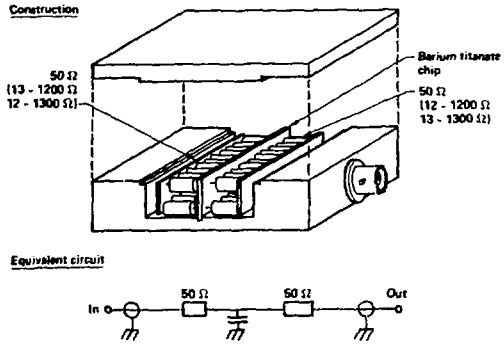

Figure 18. Sandia 50Ω, subnanosecond rise RC integrator.

frequency response can be achieved. Furthermore, the device can be used anywhere in the transmission line. The high frequency response of this design has been found to be limited to 2.8 GHz, at which frequency a resonance is observed.

Another 50 Ω integrator that has an even faster risetime has been built by Raleigh [29], who noted that the series resistors R_1 and R_2 of Fig. 17 also include stray capacitance which limit the high frequency response. The adverse effects of the stray capacitance can be minimized by adding compensating capacitors at the input and output of the integrator. A simplified method [30] is shown schematically in Fig. 19. The metal wall around the series resistors

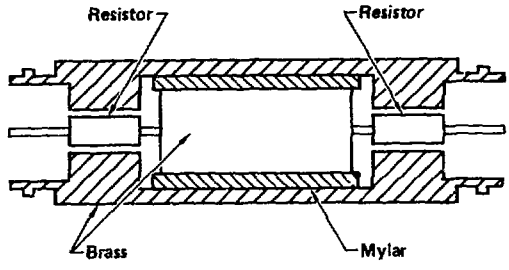

Figure 19. Simplified NRL 50Ω integrator.

provides the compensating capacitance. The brass slug separated from the wall by the mylar film is the integrating capacitor. Pulse risetimes as short as 0.2 ns and decay times of 250 ns have been measured with this device.

X-ray Wire Beam Size Measurements

Beam size measurements have been important for determining beam emittance, beam current density, and matching. The x-ray wire technique has been very useful in this respect on the ETA and ATA machines in determining beam size with 0.3 ns resolution. The technique is shown schematically in Fig. 20. It

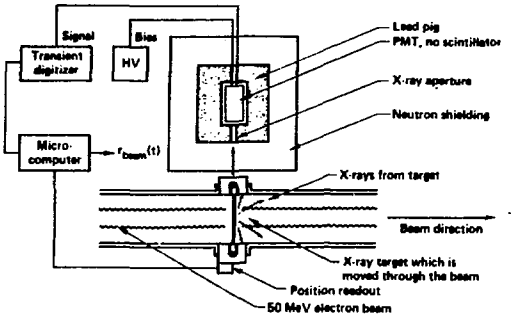

Figure 20. X-ray wire beam size measuring technique.

consists of a probe that is scanned through the beam and a detector that records the x-ray amplitude with subnanosecond resolution. The probe typically used is a tungsten powder filled graphite rod. Solid, high-Z targets will not survive multiple shots of the beam. A carbon rod is also suitable if the beam diameter is sufficiently small. The detector is a microchannelplate photomultiplier tube (Hamamatsu R1194) located in a lead pig near the beamline. The lead pig is apertured so that only x-rays from the region of the probe are allowed. For the ATA experiments it was necessary to use 300 mm of lead on the beamline and upstream sides of the detector, and 150 mm of lead on the back sides. There was an additional 3 mm thick lead filter used ahead of the detector to reduce background x-rays. The lead shielded area was also enclosed with neutron shielding that consisted of a polyethylene moderator and a borated-polyethylene thermal neutron absorber.

For each shot of the machine, the probe position and x-ray profiles are recorded and stored in a microcomputer. After the scan is completed x-ray amplitude is plotted versus probe position for each time during the beam pulse. Typical plots for four times during the pulse are shown in Fig. 21. These

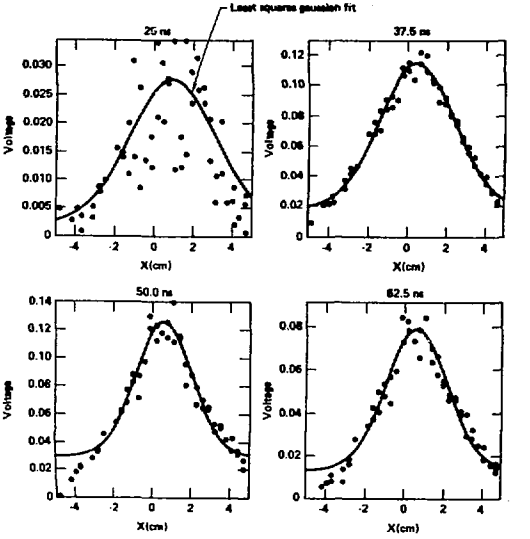

Figure 21. X-ray signal amplitude versus position for several times during the pulse.

data points are then fit to either Gaussian or Abel-inverted Bennett profiles. When this is done for all times during the pulse the result is a plot of beam size versus time, as shown in Fig. 22. This technique does require that the beam be reproducible, and that many shots be acquired.

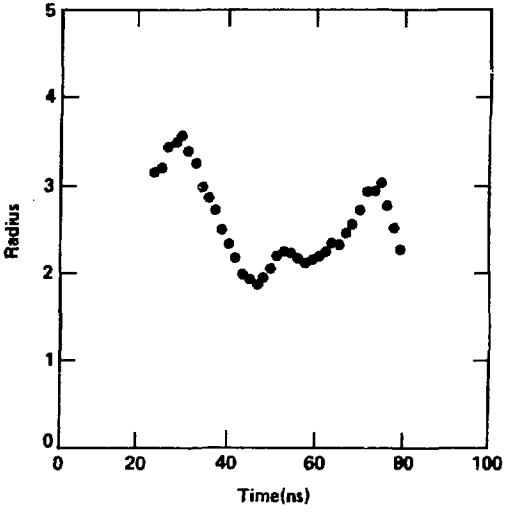

Figure 22. Beam size versus time from x-ray wire scans.

SUMMARY

A list of some of the useful electrical diagnostics used in the particle beam propagation program has been given. Most of these device are commonly used diagnostics in other programs. Unique requirements of the propagation program have motivated subnanosecond risetimes, more sensitivity, and less noise. Hopefully some of the techniques developed in this program may be of use in other programs.

*Work performed jointly under the auspices of the U.S. Department of Energy by Lawrence Livermore National Laboratory under contract W-7405-ENG-48 and for the Department of Defense under Defense Advanced Research Projects Agency ARPA Order No. 4395, monitored by Naval Surface Weapons Center under document number N60921-85-POW0001; and Naval Surface Weapons Center under document number N60921-85-WRW0201.

References

[1] R.E. Hester, et al., IEEE Trans. Nucl. Sci. NS-26, 4180 (1979); T.J. Fessenden, et al., IEEE Trans. Nucl. Sci. NS-28, 3401 (1981).

[2] L. Reginato, IEEE Trans. Nucl. Sci. NS-30, 2970 (1983).

[3] R.B. Miller, IEEE Trans. Nucl. Sci. NS-32, 3149 (1985).

[4] Y.P. Chong, et al., in Proceedings of the Fifth International Conference on High Power Particle Beams, edited by R. Briggs and A.J. Toepfter (Lawrence Livermore National Laboratory, Livermore, CA, 1984), p. 404.

[5] H.J. Kunze in Plasma Diagnostics edited by W. Lochte-Holtgreven (North-Holland, Amsterdam, 1968), pp. 603-677.

[6] V.A. J. van Lint, IEEE Trans. Nucl. Sci. NS-17, 210 (1970).

[7] J.K. Motthoff, "Coaxial Cable Responses to Ionizing Radiation from FX-100 and PR-1590 Flash X-ray Machines", McDonnell Douglas Astronautics Company-West Report No. G0436, 1970.

[8] K.W. Struve, E.J. Lauer, and F.W. Chambers, in Proceedings of the Fifth International Conference on High Power Particle Beams, edited by Richard Briggs and Alan J. Toepfler (Lawrence Livermore National Laboratory, Livermore, California, 1984), p. 408.

[9] T.F. Fessenden, Rev. Sci. Instrum. 43, 1090 (1972).

[10] J.M. White, et al., IEEE Trans. Nucl. Sci. NS-30, 2207 (1983).

[11] T.J. Fessenden, Lawrence Livermore National Laboratory Report UCID 19839, 1983.

[12] J.T. Weir, et. al., IEEE Trans. Nucl. Sci. NS-32, 1812 (1985).

[13] K.W. Struve, F.W. Chambers, and J.C. Clark, IEEE Trans. Nucl. Sci. NS-32, 1991 (1985).

[14] T.J. Fessenden, B.W. Stallard, and G.G. Berg, Rev. Sci. Instrum. 43, 1789 (1972).

[15] D. Pellinen, Rev. Sci. Instrum. 41, 1347 (1970).

[16] E.J. Lauer (private communication).

[17] T.P. Starke, Rev. Sci. Instrum. 51, 1473 (1980).

[18] C.A. Ekdahl, Bull. Am. Phys. Soc. 7, 853 (1981).

[19] S.V. Mirnov, Plasma Phys. 7, 325 (1965).

[20] K.W. Struve, "Differenced B_θ Loops for Measuring Low Level Excitations of the Beam Breakup Instability in Linear Accelerators", to be published in Rev. Sci. Instrum.

[21] C.A. Frost, C.A. Ekdahl, C.E. Crist, Sandia National Laboratory Report No. SAND84-1267C (June 1984).

[22] R.L. Carlson and L.E. Stout, IEEE Trans. Nucl. Sci. NS-32, 1956 (1985); and R.L. Carlson and L.E. Stout, "A Multi-gigahertz Beam-Current and Position Monitor for Relativistic Electron Beams", submitted to Rev. Sci. Instrum.

[23] D.G. Pellinen, et. al., Rev. Sci. Instrum. 51, 1535 (1980).

[24] V. Nassisi and A. Luches, Rev. Sci. Instrum. 50, 900 (1979).

[25] W. Stygar and G. Gerdin, IEEE Trans. Plasma Sci. PS-10, 40 (1982).

[26] C.A. Ekdahl, Rev. Sci. Instrum. 55, 1221 (1984).

[27] For example, those built by the Physics International Company, San Leandro, CA.

[28] C.A. Frost (private communication).

[29] M. Raleigh and R.E. Pechacek, Rev. Sci. Instrum. 55, 2023 (1984).

[30] M. Raleigh (private communication).